



Investigation of co-combustion characteristics of sewage sludge and coffee grounds mixtures using thermogravimetric analysis coupled to artificial neural networks modeling



Jiacong Chen, Jingyong Liu*, Yao He, Limao Huang, Shuiyu Sun, Jian Sun, KenLin Chang, Jiahong Kuo, Shaosong Huang, Xunan Ning

School of Environmental Science and Engineering, Institute of Environmental Health and Pollution Control, Guangdong University of Technology, Guangzhou 510006, China

HIGHLIGHTS

- First study on the co-combustion process of sewage sludge-coffee grounds mixtures using ANN.
- The ANN model predicted TG curves for co-combustion of mixtures with high accuracy.
- Interaction occurred and, in general, affected the decomposition in a positive manner.
- Activation energies were calculated using the KAS and OFW methods.
- The average activation energy was lowest when the mixture contained 40% coffee grounds.

ARTICLE INFO

Article history:

Received 22 August 2016

Received in revised form 4 November 2016

Accepted 16 November 2016

Available online 18 November 2016

Keywords:

Co-combustion

Sewage sludge

Coffee grounds

Thermogravimetric analysis

Artificial neural network

ABSTRACT

Artificial neural network (ANN) modeling was applied to thermal data obtained by non-isothermal thermogravimetric analysis (TGA) from room temperature to 1000 °C at three different heating rates in air to predict the TG curves of sewage sludge (SS) and coffee grounds (CG) mixtures. A good agreement between experimental and predicted data verified the accuracy of the ANN approach. The results of co-combustion showed that there were interactions between SS and CG, and the impacts were mostly positive. With the addition of CG, the mass loss rate and the reactivity of SS were increased while charring was reduced. Measured activation energies (E_a) determined by the Kissinger-Akahira-Sunose (KAS) and Ozawa-Flynn-Wall (OFW) methods deviated by <5%. The average value of E_a (166.8 kJ/mol by KAS and 168.8 kJ/mol by OFW, respectively) was the lowest when the fraction of CG in the mixture was 40%.

© 2016 Elsevier Ltd. All rights reserved.

1. Introduction

The shortage of accessible fossil fuels, and environmental problems caused by combustion of fossil fuels have increased interest in alternative and sustainable sources of energy (Lopez-Velazquez et al., 2013). Sewage sludge (SS) is the residue from the treatment process of domestic and industrial wastewater that contains many organic compounds and harmful substances (Seggiani et al., 2012). In its dry form, SS is one of the potential options for an alternative fuel because of the high quantity of organic matter with sufficiently high calorific value, similar to that of brown coal (Garcia et al., 2013; Magdziar

and Werle, 2014). There are several thermal technologies for the recovery of useful forms of energy from sewage sludge, such as pyrolysis, gasification, combustion and co-combustion processes (Manara and Zabaniotou, 2012; Jayaraman and GökalpZhou, 2015). Biomass is considered a clean, renewable and environmentally friendly energy resource that contributes to the reduction of net CO₂ emission (Du et al., 2014; Gil et al., 2015). It is often used to increase the volatile matter content and provide a more stable flame during the co-combustion process. Although the low density of biomass does result in escape from the combustion zone, the high heating value and the low ash content compared to SS tends to reduce waste and increase efficiency. Therefore, the co-combustion of SS and biomass could avoid the disadvantages of each and improve the overall combustion efficiency.

* Corresponding author.

E-mail addresses: www053991@126.com, Liujiy@gdut.edu.cn (J. Liu).

Coffee is a popular drink prepared from roasted coffee beans, with global production of approximately 500 billion cups per annum (Li et al., 2014). Vast quantities of byproduct called coffee grounds (CG) are obtained from the treatment of coffee to make the powder that is mixed with hot water to prepare instant coffee. Annually the amount of CG is gradually increasing with growth in coffee consumption (Jeguirim et al., 2014). These residues have no significant market and due to their large volume they also cause a storage and disposal problem (Li et al., 2014). Currently, combustion is the simplest and most direct technology in utilization of biomass, amounting to more than 97% of total global bio-energy production (Peng et al., 2015). In this work, the potential of CG as a blending biomass is studied to explore the possibility of technological breakthroughs. Thermogravimetric analysis (TGA) has been widely used to investigate co-combustion characteristics (Peng et al., 2015; Toptas et al., 2015). Numerous studies involving the analysis of co-combustion have been reported (Sahu et al., 2014; Goldfarb and Ceylan, 2015). However, there is limited research concerning the co-combustion process of CG and SS and their interaction is unclear (Liu et al., 2015). Additionally, in these studies some complex multistep reactions during the co-combustion process have handicapped the development of conventional empirical modeling based on linear and statistical approaches. These models have failed to confirm three kinetic parameters simultaneously and explain the complexity of co-combustion phenomena.

Artificial intelligence techniques such as artificial neural networks (ANNs) can be used for complex problems in a non-linear fashion to attain high operational performance, and (once trained) can be applied for anticipation and generalization at high speed (Rivera et al., 2010; Vani et al., 2015). The basic processing elements of ANNs are interconnected neurons that create a structure to form a process prediction model. The effectiveness of ANN models in the prediction of process parameters relating to energy-related processes have been demonstrated (Mikulandric et al., 2014; Ata, 2015; Gajic et al., 2015; Sahin, 2015), but the potential to estimate parameters of the co-combustion processes of CG with SS have not been studied.

In this study, the combustion characteristics of SS, CG and their blends were investigated by TGA at three different heating rates (10, 20 and 30 °C·min⁻¹) and mixing ratios. Knowledge of the co-combustion characteristics of sludge-biomass blends, in particular, accurate estimation of thermal behavior, is essential to achieving effective design and operation of industrial systems (Celaya et al., 2015). Thus, this study is directed towards developing an ANN model to accurately predict the thermal behavior of multistep co-combustion reactions of SS-CG. Furthermore, activation energies (E_a) for the fuel materials were analyzed by the Kissinger-Akahira-Sunose (KAS) and the Ozawa-Flynn-Wall (OFW) methods.

2. Materials and methods

2.1. Materials

A sample of SS was collected from an urban wastewater treatment plant located in Guangzhou, China. CG was collected from an instant coffee processing factory in China. Both materials were air-dried and ground in a grinder, then sieved to obtain particles less than 74 μm in diameter. All of the samples were dried in oven at 105 °C for 24 h and stored in a desiccator. Mixture samples of SS-CG were prepared at mixing ratios of 9:1, 8:2, 7:3 and 6:4 on a weight basis, and were named SC91, SC82, SC73, SC64, respectively. The proximate and ultimate analyses of SS and CG samples are shown in Table 1.

2.2. Thermogravimetric analysis (TGA)

Non-isothermal experiments were conducted with a TG analyzer (NETZSCH STA 409 PC Luxx, Germany). Each sample (10 ± 0.5 mg) was heated from room temperature to 1000 °C at three different heating rates of 10, 20 and 30 °C·min⁻¹ in air with a flow rate of 50 ml·min⁻¹. Each experiment was replicated three times to ensure reproducibility, and the errors of experimental results were within ±2%.

2.3. ANN model development

There are different types of training algorithms for ANN, such as Leven-Marquardt (LM) (Vani et al., 2015; Yildiz et al., 2016), gradient descent momentum (GDM), adaptive learning rate (GDx) (Buyukada, 2016), scaled conjugate gradient (SCG) and Broyden-Fletcher-Goldfarb-Shanno quasi-Newton (BFGS) (Pandey et al., 2016). In this study, LM algorithm is chosen since it often has higher rates of convergence than the other algorithms (Yildiz and Uzun, 2015). A multi-layer perception (MLP) based feed forward ANN with a Leven-Marquardt back propagation algorithm is used to predict the TG curves of SS-CG blends. This ANN is the most widely used for optimization studies because of its simplicity and high accuracy (Mazrou, 2009). The MLP networks consist of an input layer, two hidden layers and an output layer (Fig. 1). In the MLP, all layers were interconnected by weights and biases that adjusted it to model non-linear functions. In this framework, the heating rate, mixing ratio and temperature-dependent mass loss percent were used as the input vectors. Hidden layers were employed to implement complex and non-linear functions in the model (Vani et al., 2015). The number of hidden layers, number of neurons and training epochs were reset and fixed in terms of root mean square error (RMSE), mean absolute error (MAE), mean bias error (MBE) and coefficient (R^2), by trial and error until the optimal ANN architecture was obtained. These errors were evaluated by Eqs. (1)–(3).

$$\text{RMSE} = \sqrt{\frac{1}{N} \sum_{i=1}^N (H_i - H_{i,\text{model}})^2} \quad (1)$$

$$\text{MAE} = \frac{1}{N} \sum_{i=1}^N |H_i - H_{i,\text{model}}| \quad (2)$$

$$\text{MBE} = \frac{1}{N} \sum_{i=1}^N (H_i - H_{i,\text{model}}) \quad (3)$$

Lower values of both RMSE and MAE and higher values of R^2 indicate better ANN models for the training data. The ANN model was performed using the ANN toolbox available in Matlab.

2.4. Kinetic theory

Kinetic equation for the thermal decomposition processes of the different constituents is expressed based on rate of conversion as follows:

$$\frac{d\alpha}{dt} = k(T)f(\alpha) \quad (4)$$

where t (min) is time, T is the absolute temperature, $f(\alpha)$ represents the function of reaction mechanism, and α is the degree of conversion that can be calculated as:

Table 1
The proximate analyses, ultimate analyses and heat value of SS and CG sample on air dried basis.

Sample	Ultimate analyses (wt.%)					Proximate analyses (wt.%)				$Q_{net,d}^a$ (MJ·kg ⁻¹)
	C	H	O ^f	N	S	M ^b	V ^c	A ^d	FC ^{e,f}	
SS	34.04	5.03	23.48	6.09	1.67	5.50	48.80	43.38	2.32	12.02
CG	56.94	15.23	20.88	2.76	0.98	2.69	74.82	0.56	21.93	21.30

^a $Q_{net,d}$, lower heating value on dry basis.

^b M, moisture.

^c V, volatile matters.

^d A, ash.

^e FC, fixed carbon.

^f O and FC, Calculated by difference.

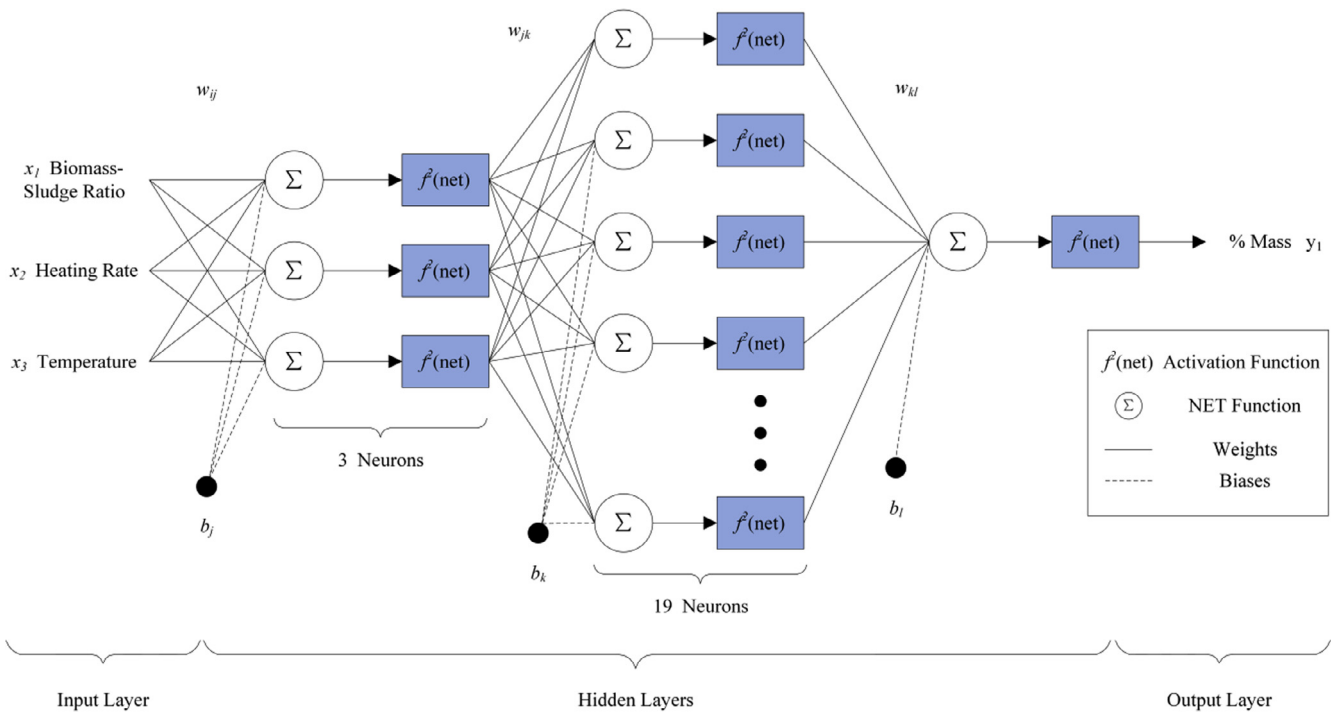


Fig. 1. Optimal ANN structure used for predicting co-combustion behavior of different SS-CG mixtures.

$$\alpha = \frac{W_0 - W_i}{W_0 - W_f} \quad (5)$$

where W_0 , W_i and W_f stand for initial, instantaneous, final masses, respectively.

$k(T)$ is temperature dependent rate constant as expressed by Arrhenius Law as:

$$k(T) = A \exp\left(-\frac{E_a}{RT}\right) \quad (6)$$

where A is the pre-exponential factor, E_a (J·mol⁻¹) is the activation energy of the reaction, R is the universal gas constant, 8.314 J·mol⁻¹·K⁻¹. By substituting Eq. (3) in Eq. (1) gives:

$$\frac{d\alpha}{dt} = A e^{\left(-\frac{E_a}{RT}\right)} f(\alpha) \quad (7)$$

Taking into account that the temperature is a function of time and that it is increasing with the constant heating rate β (K·s⁻¹), then β is written below:

$$\beta = \frac{dT}{dt} = \frac{dT}{d\alpha} \frac{d\alpha}{dt} \quad (8)$$

Eqs. (7) and (8) can be combined and rearranged to give:

$$g(\alpha) = \int_0^\alpha \frac{d\alpha}{f(\alpha)} = \int_0^T \frac{A}{\beta} e^{-E_a/RT} dT = \frac{AE_a}{\beta R} \int_x^\infty u^{-2} e^{-u} du = \frac{AE_a}{\beta R} P(x) \quad (9)$$

where $x = E_a/RT$, the function $P(x)$ has no exact solution, hence Eq. (9) can be solved by numerical methods or approximations. The name of iso-conversional methods differs by the type of approximation method used.

In this study, two kinds of iso-conversional methods, Kissinger-Akahira-Sunose (KAS) and Flynn-Wall-Ozawa (FWO) were applied to calculate the activation energy (E_a).

The KAS method (Kissinger, 1957; Akahira and Sunose, 1971) uses approximation of $P(x) = x^{-2} e^{-x}$ to Eq. (9). After rearrangement, the equation is shown below:

$$\ln\left(\frac{\beta}{T^2}\right) = \ln\left(\frac{AE_a}{Rg(\alpha)}\right) - \frac{E_a}{RT} \quad (10)$$

where the plot of $\ln(\beta/T^2)$ against $1/T$ gave a straight line from which the slope can be used to determine the E_a .

The FWO method (Ozawa, 1965; Flynn and Wall, 1966) was derived from Doyle's approximation (Doyle, 1961) with Eq. (9), the equation becomes:

$$\ln \beta = \ln \left(\frac{AE_a}{Rg(\alpha)} \right) - 5.331 - 1.052 \frac{E_a}{RT} \quad (11)$$

where the value of E_a for different conversion values can be calculated from the slope of $\ln \beta$ versus $1/T$.

3. Results and discussion

3.1. Combustion process of the pure materials

TG and DTG curves of pure materials obtained at a heating rate of $20 \text{ }^\circ\text{C}\cdot\text{min}^{-1}$ are shown in Fig. 2. There are remarkable differences in the combustion behavior for both pure samples. The

combustion process of SS was divided into two phases. The first decomposition phase occurs in the range of $180\text{--}395 \text{ }^\circ\text{C}$ and the second in $395\text{--}640 \text{ }^\circ\text{C}$. These two phases are caused primarily by the decomposition of carbohydrates and lipids (Magdziarz and Werle, 2014). After these processes, 52% of the total mass was degraded. The thermal degradation of the CG involved two discrete phases. A main devolatilization zone occurs between $150 \text{ }^\circ\text{C}$ and $335 \text{ }^\circ\text{C}$ due to the oxidative degradation of hemicellulose and cellulose (Yang et al., 2006; Zhou et al., 2013). The second occurs in the $410\text{--}475 \text{ }^\circ\text{C}$ temperature range where the thermal degradation is closely related to the lignin decomposition and the combustion of char (Jeguirim et al., 2014). In fact, a shoulder at $448 \text{ }^\circ\text{C}$ appears on the right of the second decomposition peak. This behavior is due

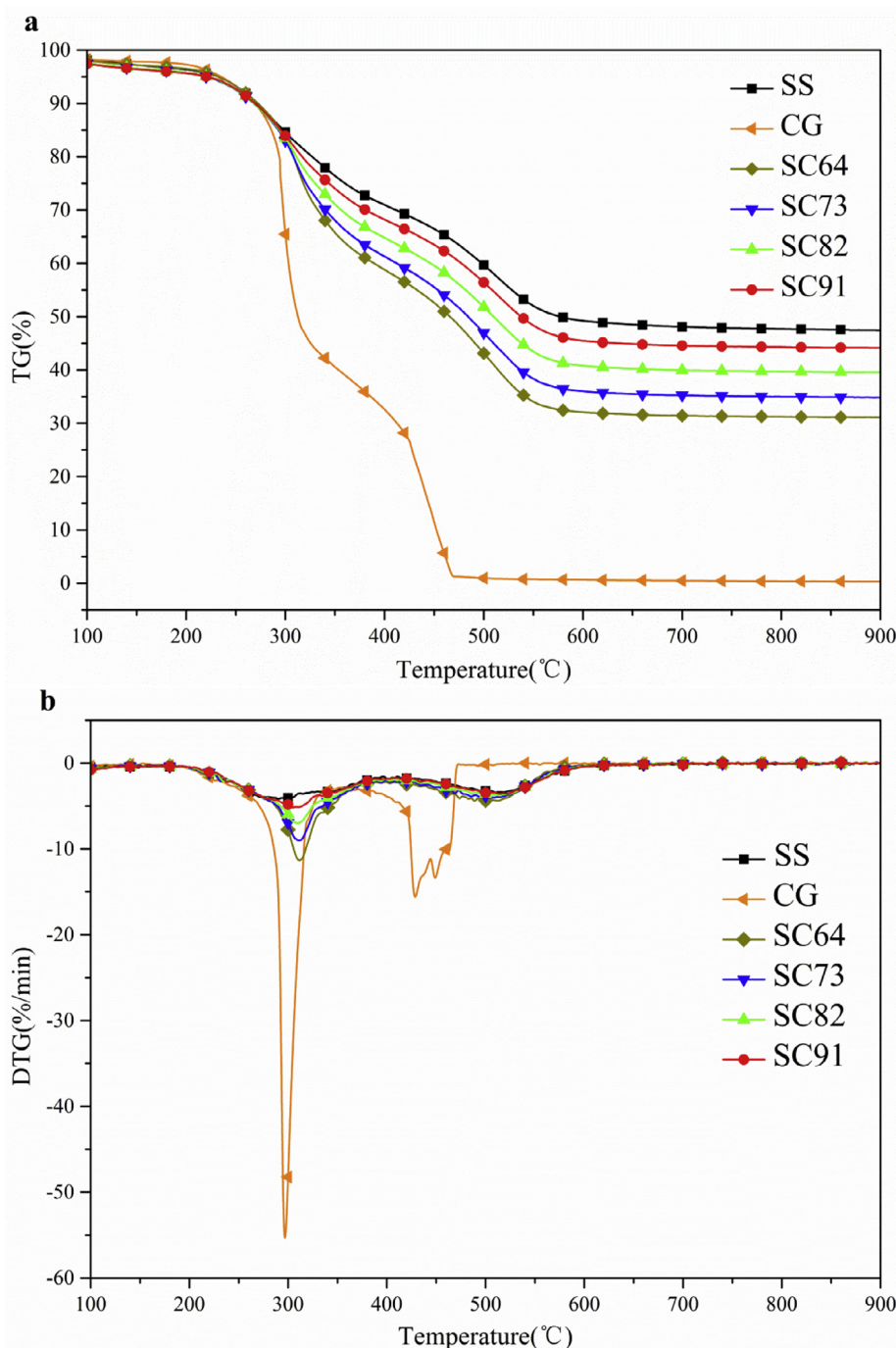


Fig. 2. TG(a) – DTG(b) curves of SS, CG and their mixtures at the heating rate of $20 \text{ }^\circ\text{C}\cdot\text{min}^{-1}$.

to the higher lignin content of the CG that degrades over a wide temperature range from 160 to 900 °C (Yang et al., 2006).

Comparison of SS and CG thermal degradation shows that the maximum mass loss rate (DTG curves) of CG is higher than for SS. This can be attributed to the release of volatile matter in the CG that burns more quickly and intensely. The maximum temperature in the DTG curves of CG appears at a higher temperature, 296 °C, than for SS, 290 °C. The reason for this phenomenon is that the CG is composed of a mixture of galactomannans, cellulose and arabinogalactans, confirming higher inter-chain hydrogen bonds and ordered structure (Simões et al., 2014).

3.2. Co-combustion of SS-CG blends

The TG and DTG profiles of the SS-CG mixture samples at the heating rate of 10 °C·min⁻¹ are displayed in Fig. 2 and lie between the profiles of the pure samples. In the DTG curves of the mixtures, two oxidation stages can be observed. The first one at temperatures of 160 °C and 385 °C, corresponds to the hemicellulose and cellulose decomposition. In the second stage, up to ~585 °C, a broader peak is present, which is due to the release of volatile matter in the SS that burns slowly over the whole temperature range, together with the char. To investigate the combustion characteristic of SS and CG, the comprehensive combustion index *S* is defined as follows (López-González et al., 2014):

$$S = \frac{(dW/dt)_{\max}(dW/dt)_{\text{mean}}}{T_i^2 T_f} \quad (12)$$

where $(dW/dt)_{\max}$ refers to the maximum mass loss rate, $(dW/dt)_{\text{mean}}$ is the average mass loss rate, T_i is the ignition temperature and T_f is the burnout temperature. The bigger the index *S* is, the more vigorously the samples burned and the quicker char burned out.

The co-combustion characteristic parameters of the SS-CG mixtures are shown in Table 2. As observed in Table 2, the ignition temperature (T_i) and the burnout temperature (T_f) of CG are 289.1 °C and 466.4 °C, and the T_i and the T_f of SS are 240.6 °C and 675.6 °C. The T_f of CG is lower 209.2 °C than SS. This finding shows that SS contains more nonflammable material than CG. Although the volatile matter of CG is higher than that of SS, the T_i of SS is lower 48.5 °C than CG that can primarily be attributed to differences in composition and structure. SS is composed of lower organic matter, such as humic acids, fulvic acids and polycyclic aromatic hydrocarbon (Kulikowska, 2016; Oleszczuk, 2009). These compounds have a simple structure and have been broken down by biological oxidation. As a result, these organisms are easy to decompose at high temperature. In contrast, CG is primarily formed by proteins, carbohydrate and lipid (López-Barrera et al., 2016) that are macromolecular organic compounds with complex structures. Therefore, CG needs more energy and higher tempera-

ture to break the chemical bonds. The residue mass percentages of CG and SS are 0.25% and 47.23% that are almost consistent with the ash content in Table 1.

Fig. 3 presents the tendency of T_i , T_f , T_m , M_f , DTG_{\max} and *S* according to the mixtures with different CG fractions (10–40 wt. %). The columns for the T_i , T_m , DTG_{\max} and *S* reveal an increasing trend as the CG proportion increases while T_f and M_f show a decreasing trend. From Fig. 3a and c, the ignition temperature (T_i) and the peak temperature (T_m) are not linear with the increase of CG but have an exponential relationship, with the values of R^2 close to 1 and 0.9951, respectively. As seen in Table 2, the T_m for the mixture are higher than for pure SS and CG indicating the presence of interaction between the fuels composing. The maximum slope of the fitting curves occur when the CG proportion is below 20% and declines gradually with the increase of CG content, hinting at a decreasing trend in the intensity of the suppressive effect. As exhibited in Fig. 3b and e, the burnout temperature (T_f) and the residual mass (M_f) are linearly proportional to the CG content, their correlation coefficients (R^2) are as high as 0.9571 and 0.9958, respectively. Moreover, the T_f value of the mixture sharply decreases 51 °C when CG = 10 wt.%. Such phenomenon indicates that the addition of CG might improve the burnout of SS.

The DTG_{\max} shows a strong linear trend with the CG content and its R^2 is 0.9959. It can be seen that an increase of the CG fraction in the mixture raises the intensity of the first peak, which suggests that the higher proportion of CG, the higher reactivity of the mixture (Zheng and Koziński, 2000). Fig. 3f shows that the index *S* has an exponential relationship with the proportion of CG and its R^2 is 0.9998. As shown in Table 2, the index *S* of CG is much higher than that of SS. Increasing CG content in the mixture causes the value of the index *S* to increase from 1.192×10^{-7} to $32.109 \times 10^{-7} \text{ min}^{-2} \cdot \text{°C}^{-3}$. When the value of the comprehensive combustion characteristic index *S* is greater than 2, it could be considered as a good general combustion performance (Parshetti et al., 2014). It is observed that when CG fraction in the mixture is more than 20 wt.%, the index *S* is greater than 2. This suggests that the blending of CG can enhance the combustion performance of SS. These results are due to the high volatile matter/(volatile matter + fixed carbon) ratio and high carbon content of CG (Parshetti et al., 2014). Therefore, the mixture burns out much earlier and the combustion characteristics of the mixture improve with an increase of the CG ratio.

3.3. Interaction investigation of co-combustion for SS-CG mixtures

The superposition property was applied to investigate whether there is an interaction between SS and CG during the mixture decomposition, where the theoretical TG/DTG curves of mixture Y_{mix} can be calculated based on the mass fraction of single components (Aboulkas et al., 2008):

Table 2
Combustion characteristic parameters of SS, CG and their mixtures.

Samples	T_i^a (°C)	T_f^b (°C)	T_m^c (°C)	DTG_{\max}^d (%/min)	M_f^e (%)	S^f (10^{-7})
SS	240.6	675.6	290.3	-4.15	47.23	1.192
SC91	250.8	624.6	304.7	-5.16	44.02	1.577
SC82	264.0	607.3	309.6	-6.98	39.49	2.145
SC73	272.6	600.8	311.3	-9.01	34.70	2.830
SC64	278.4	582.6	311.5	-11.32	31.02	3.727
CG	289.1	466.4	296.8	-55.30	0.25	32.109

^a T_i , the ignition temperature.

^b T_f , the burnout temperature.

^c T_m , the peak temperature.

^d DTG_{\max} , the maximum mass loss rate.

^e M_f , the residual mass.

^f *S*, the comprehensive combustion index, unit is $\text{min}^{-2} \cdot \text{°C}^{-3}$.

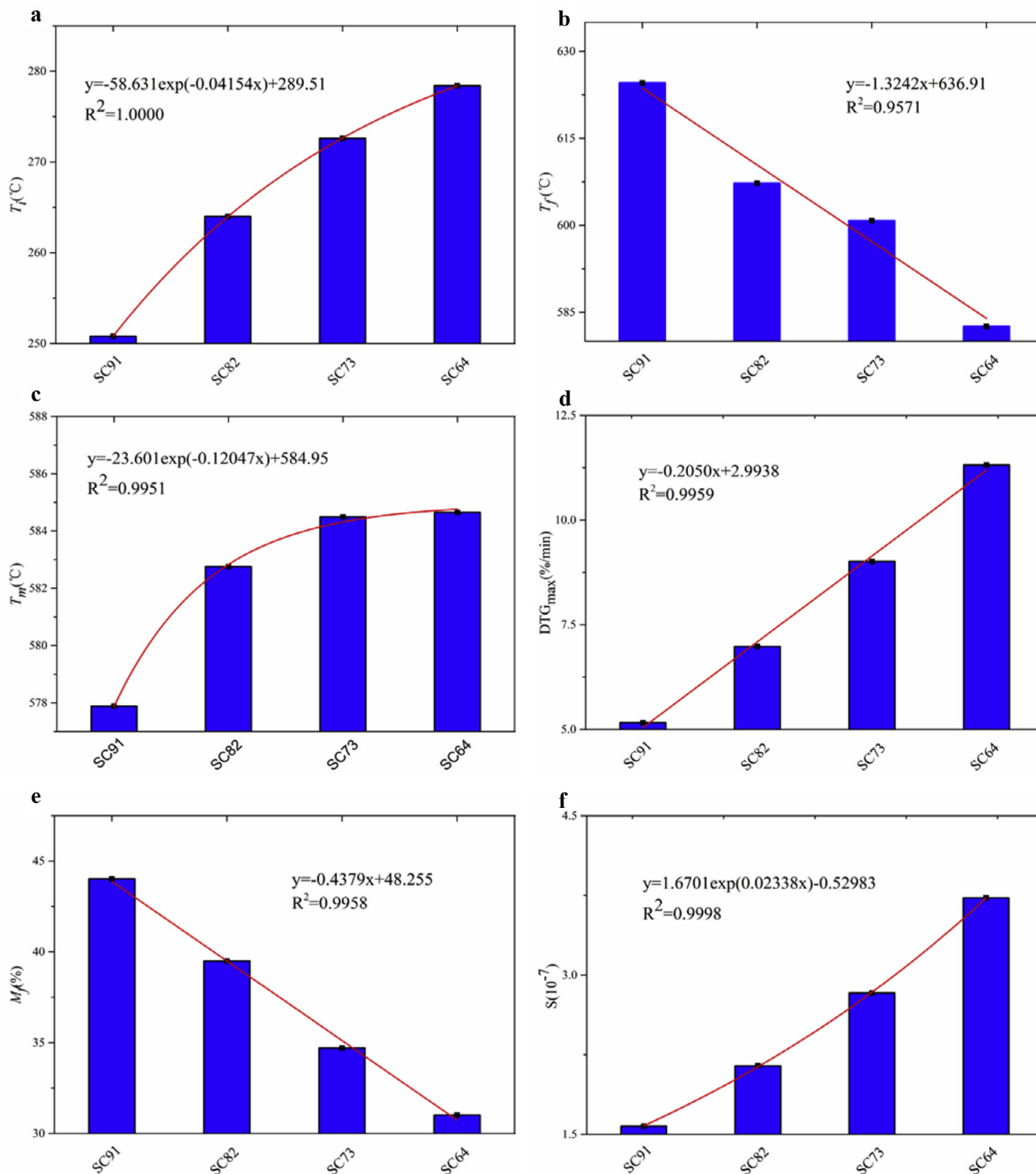


Fig. 3. The relationship between T_f (a), T_f (b), T_m (c), DTG_{max} (d), M_f (e) and S (f) and CG fractions (10–40 wt.%) in the mixture.

$$Y_{mix} = f_1 Y_{SS} + (1 - f_1) Y_{CG} \quad (13)$$

where the coefficients f_1 and $(1 - f_1)$ are the mass fractions of SS and CG at any temperature, Y_{SS} or Y_{CG} is the TG/DTG of the pure sample experiencing a process in the same operational conditions as the mixture. ΔW ($\Delta W = TG_{experimental} - TG_{calculated}$) is introduced as the difference of mass remaining between the experimental data and the calculated values to explicitly interpret the interaction and the results are depicted in Fig. 4b. Thus, values of ΔW that are

positive or negative may indicate catalysis on solid phase and promotion in devolatilization, respectively.

The calculated TG/DTG curves of SC64 are depicted in Fig. 4a based on the measured TG/DTG curves of the pure constituents. It can be seen that the calculated curve matches the experimental one at the initial stage. As exhibited in Fig. 4b, the value of ΔW remains approximately zero at this stage meaning that the interaction between SS and CG is not obvious at low temperature. Subsequently, ΔW first increases at 252 °C and reaches the first peak (ΔW_{max1}) at 308 °C then decreases until 389 °C. The value of ΔW

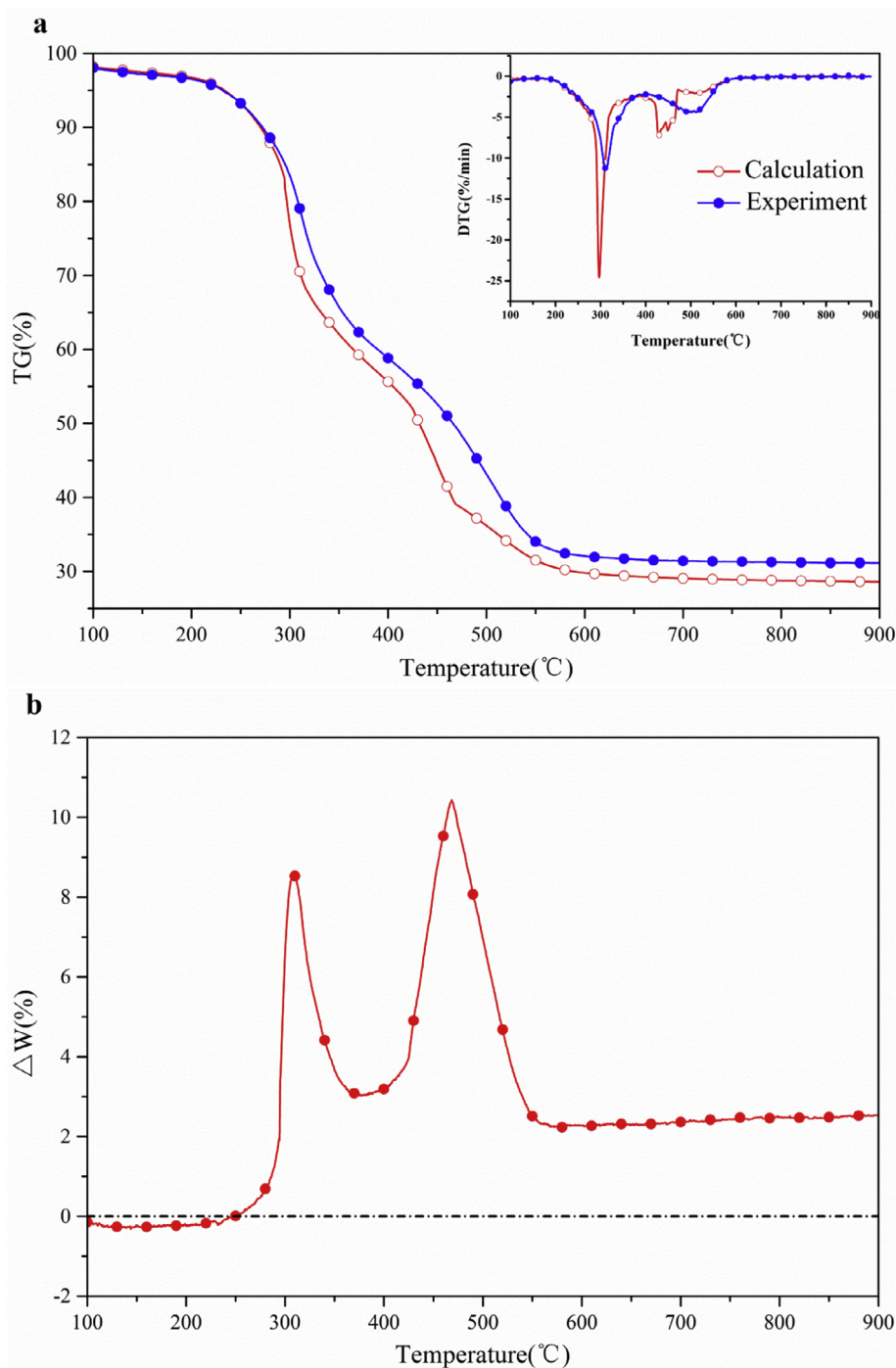


Fig. 4. (a) Experimental and calculated TG/DTG curves of SC64 at 20 °C·min⁻¹; (b) ΔW of SC64.

increases again when reaching the second peak (ΔW_{max2}) at 468 °C and then decreases again. This decrease ends at 556 °C where a plateau appears with a height of approximately 2.3% that is maintained until the end.

From Fig. 4a, it can be seen that a shift of the experimental DTG curve compared to the calculated curve occurs at the main decomposition region. The maximum mass loss rate in the experiment is much lower than the calculation, suggesting a suppressive effect of the interactions on devolatilization. If there are no interactions during the co-combustion processes, the DTG peaks present in the temperature range of 400–620 °C should occur separately at 430 °C, 450 °C and 520 °C – with a shoulder at 450 °C attached

on the right of the DTG peak at 430 °C. When the SS and CG are mixed, there is only one peak for SC64, which implies the existence of interactions in this stage and that the reactions in relation to mineral decomposition, carbonaceous residue thermal cracking and gasification occur simultaneously rather than in series (Duan et al., 2009; He et al., 2015). The experimental DTG values are larger, for the most part, than those obtained by calculation at approximately 465–620 °C, suggesting that the interactions might facilitate gasification. Presently, the mechanism of the interactions in decomposition of the SS and CG mixture is seldom studied. Previous research has found that after removing the mineral matter of paper mill sludge, the maximum mass loss rate and the peak

temperature increase significantly (Vamvuka et al., 2009; Peng et al., 2015). Therefore, the interaction could be interpreted as char and gas evolved from the CG decomposition reacting with the SS residue. When the CG as the additive is blended, it could release more heat to accelerate the endothermic reaction, promoting the decomposition and combustion of the residue, but components in the SS may restrain the interaction and lead to greater charring.

3.4. Effect of heating rate

Typical TG and DTG curves at different heating rates (10, 20 and 30 °C·min⁻¹) for the SC64 sample are demonstrated in

Fig. 5. The heating rate had a significant effect on the combustion behavior of the mixture samples, where the positions of the peaks shift to the right with increased heating rates. The maximum peaks of conversion are 302, 311 and 316 °C for heating rates of 10, 20 and 30 °C·min⁻¹. This phenomenon is common for non-isothermal heating (Kan et al., 2014a,b; Lin et al., 2010). It could be due to the heat conduction of the particles that can result in heat diffusion. At a low heating rate, the heating of samples occurs more gradually and result in better heat transfer from the surface to the inner portion, generating a narrow temperature gradient across the particles. At a high heating rate, the relatively steep temperature gradient leads to a lag of reactions (Kan et al., 2014a,b).

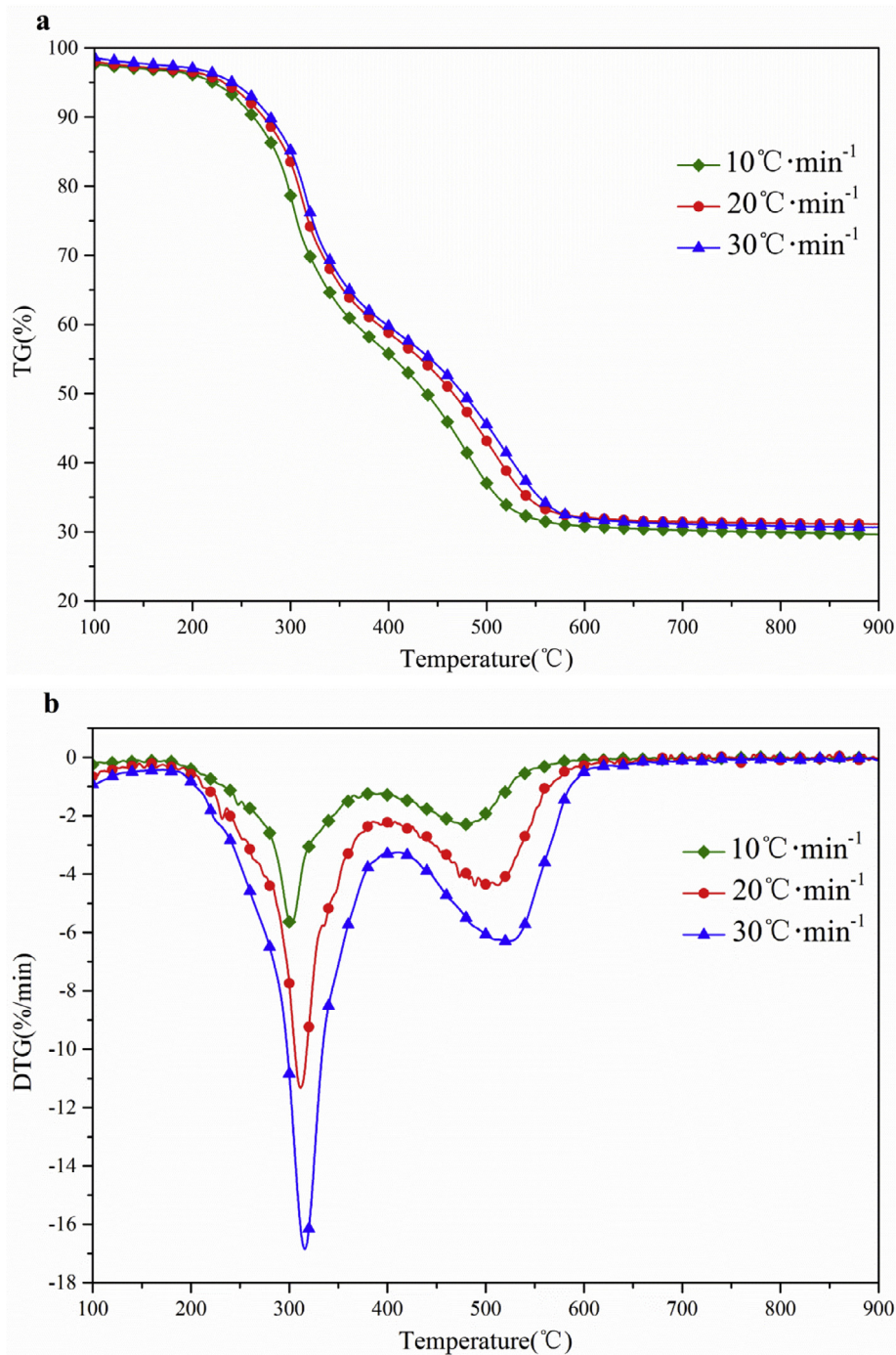


Fig. 5. TG(a) – DTG(b) profiles of SC64 at different heating rates.

Table 3
Comparison of different ANN network structure performances.

Model	Inputs	Network topology	RMSE	MBE	MAE	R ²
ANN1	Mixture ratio, heating rate, temperature	3*1	5.178	-3.125	4.266	0.9808
ANN2		5*1	5.018	-3.144	4.137	0.9819
ANN3		7*1	3.012	1.651	2.316	0.9943
ANN4		11*1	4.395	3.580	3.789	0.9927
ANN5		13*1	7.687	7.103	7.103	0.9794
ANN6		15*1	8.972	7.928	7.928	0.9734
ANN7		17*1	7.192	2.737	5.710	0.9776
ANN8		19*1	7.074	3.505	5.625	0.9791
ANN9		3*3*1	3.263	-1.091	2.443	0.9922
ANN10		3*5*1	4.393	-2.754	3.618	0.9920
ANN11		3*7*1	3.165	-2.144	2.413	0.9837
ANN12		3*11*1	1.848	0.997	1.121	0.9985
ANN13		3*13*1	6.203	5.030	5.185	0.9856
ANN14		3*15*1	0.792	-0.200	0.680	0.9997
ANN15		3*17*1	2.179	1.283	1.650	0.9980
ANN16		3*19*1	0.482	0.243	0.371	0.9999
ANN17		5*3*1	0.866	0.425	0.582	0.9996
ANN18		5*4*1	4.395	2.493	3.200	0.9902
ANN19		5*8*1	3.576	-1.345	2.705	0.9944
ANN20		5*10*1	3.073	-1.557	2.403	0.9961

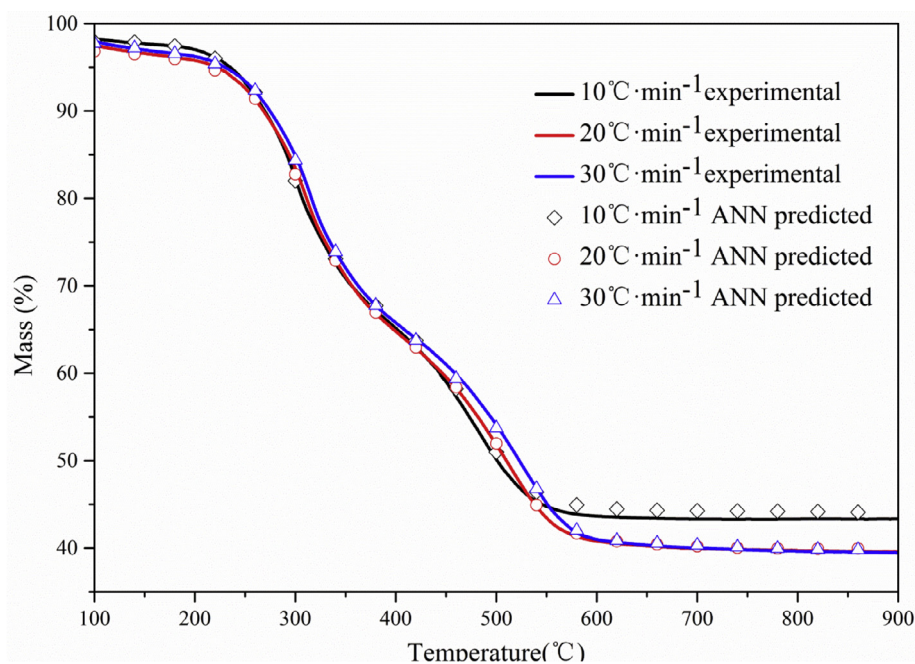


Fig. 6. Comparisons of testing performance of ANN16 model for SC82 at different heating rates.

3.5. ANN model for co-combustion of SS-CG blends

The combustion data are divided into two groups with 80% used for training and 20% used for testing. Different ANN configuration performances with a resetting of hidden layers and neurons based on the LM algorithm are presented in Table 3. Total training epochs (iterations) of the model are set to 2000 and the performance goal is 10^{-5} . Linear (purelin), log-sigmoid (logsig) and hyperbolic tangent-sigmoid (tansig) functions are the three most commonly used transfer functions. The selection of a suitable function can be conducted by considering influencing factors such as the degree of complexity of the problem, the node numbers of the training group, and the bias and weight of the net to achieve the most rapid convergence (Caner et al., 2011). In this network topology, the activation function of neurons in the input layer and hidden layers is assumed as a tansig function, and the activation function of neu-

rons in the output layer is assumed as a pure linear (purelin) function (Yildiz et al., 2016). From Table 3, the ANN16 provided the lowest RMSE value. As seen from Fig. S1, the values of the regression coefficients of this network were 0.9999 and 0.9998 for training and testing, respectively. Therefore, the ANN16 was chosen as the suitable model and used to simulate the mass loss percent for the rest of the mixing ratios. The structure of ANN16 is shown in Fig. 2. The ANN14 architecture consisted of four layers: an input layer with 3 input parameters (mixing ratio, heating rates and temperature), two hidden layers, the first one with 3 and the second with 19 hidden neurons, and an output layer with 1 output parameter-mass loss percent ($3 \times 19 \times 1$). Predictions of the mass percent with the ANN16 network as a function of the measured results are shown in Fig. 6. The agreement between the experimental and predicted TG curves confirmed the predictive power of the ANN modeling.

Table 4
 E_a and corresponding R^2 of SS and SS/CG mixture in air by KAS and OFW methods.

Samples	α	KAS method		OFW method	
		E (kJ/mol)	R^2	E (kJ/mol)	R^2
SS	0.2	207.34	0.9685	205.83	0.9711
	0.3	227.39	0.9875	225.32	0.9885
	0.4	223.94	0.9975	222.53	0.9977
	0.5	174.89	0.9991	176.47	0.9992
	0.6	128.58	0.9963	133.35	0.9970
	0.7	135.75	1.0000	140.89	1.0000
	0.8	139.74	1.0000	145.20	1.0000
	Average	176.80		178.51	
SC64	0.2	181.19	0.9995	181.18	0.9995
	0.3	198.78	0.9971	198.19	0.9974
	0.4	197.66	0.9966	197.36	0.9969
	0.5	178.28	0.9996	179.36	0.9996
	0.6	134.80	0.9987	138.81	0.9989
	0.7	136.99	1.0000	141.72	1.0000
	0.8	139.83	0.9998	145.00	0.9998
	Average	166.79		168.80	
SC73	0.2	222.18	0.9609	220.10	0.9639
	0.3	218.38	1.0000	216.81	1.0000
	0.4	214.21	0.9944	213.10	0.9949
	0.5	174.44	0.9966	175.74	0.9969
	0.6	117.71	1.0000	122.58	1.0000
	0.7	123.00	0.9982	128.43	0.9984
	0.8	127.50	0.9977	133.29	0.9980
	Average	171.06		172.86	
SC82	0.2	263.65	0.9662	259.47	0.9684
	0.3	233.22	0.9979	230.90	0.9981
	0.4	217.69	0.9982	216.45	0.9983
	0.5	168.76	0.9990	170.40	0.9991
	0.6	118.22	0.9992	123.18	0.9994
	0.7	123.07	0.9999	128.61	0.9999
	0.8	120.93	0.9981	127.12	0.9984
	Average	177.94		179.45	
SC91	0.2	244.83	0.9628	241.51	0.9654
	0.3	221.02	0.9910	219.27	0.9917
	0.4	209.79	0.9998	208.98	0.9998
	0.5	155.85	0.9997	158.22	0.9998
	0.6	109.89	0.9996	115.38	0.9997
	0.7	117.98	0.9984	123.85	0.9986
	0.8	119.56	0.9982	125.90	0.9985
	Average	168.42		170.45	

3.6. Kinetic analysis

According to Eqs. (10) and (11), the activation energies (E_a) of several conversions (α) can be determined from the slope of a straight line obtained from a plot of $\ln(\beta/T^2)$, $\ln \beta$ against $1/T$. The heating rates of 10, 20 and 30 °C·min⁻¹ were used to estimate E_a by iso-conversional KAS and OFW models within $\alpha = 0.2$ – 0.8 . The E_a values and the corresponding determination coefficients (R^2) for SS and SS-CG mixtures are listed in Table 4. As shown in Table 4, all the values of R^2 are equal to or greater than 0.96 meaning that the KAS and OFW models are well correlated with the combustion process.

In this analysis, the E_a values corresponding to the designated α are the average values of reactions at each point in α because the thermal decomposition of samples involved various complex reactions that are difficult to analyze separately (Kim et al., 2010). The values of E_a obtained by the KAS and OFW methods are very similar with a deviation below 5%, indicating the reliability of calculations using these two methods (Lopez-Velazquez et al., 2013). Activation energy is the minimum energy required to start a chemical reaction and a higher E_a value means a more difficult reaction is generated. E_a can also be used to determine the reactivity and sensitivity of a reaction (Gai et al., 2013).

Kinetic analysis results show that E_a is highly dependent on α , which implies that SS and CG co-combustion is a complex process

consisting of different reactions. For the KAS model, the E_a value of SS increases from 0.2 to 0.3 conversion and decreases between 0.3 and 0.6 conversion then raises after 0.6 conversion. A similar trend was also observed in the OFW model. In respect to the mixtures, it is important to note that SC64 has the lowest E_a values from the 0.2 to 0.4 conversions suggesting that the 40 wt.% CG portion facilitates the devolatilization reaction of the mixture at low temperature. However, after the 0.4 conversion, SC64 obtains the highest value followed by SS and SC91, revealing a suppressive and accelerative impact of the 40 and 10 wt.% CG fractions on the mixture decomposition at high temperature. From Table 4, an explicit comparison of the average of E_a for mixtures by both methods can be made. SC64 obtains the lowest average E_a that is 166.8 kJ/mol calculated by KAS and 168.8 kJ/mol obtained by OFW. Furthermore, the E_a average of SC64 is lower than SS, implying a synergistic effect between the components of the mixture that can potentially be attributed to the influences of char within SS on the decomposition of CG. This finding is in agreement with the results obtained from the analysis of DTG_{max} that suggest that the presence of CG improves the reactivity of the mixture. Ceylan and Topçu (2014) studied the kinetic mechanism of hazelnut husk and calculated E_a values between 95 and 162.1 kJ/mol. Damartzis et al. (2011) reported that the E_a values for cardoon stems and cardoon leaves are 224.1 kJ/mol and 350.07 kJ/mol. Peng et al. (2015) examined the thermal kinetics of textile dyeing sludge-microalgae blends

and reported that the minimal value is 227 kJ/mol. This study is the first report on the co-combustion kinetics of SS-CG blends and the calculated average value of E_a for SS-CG mixtures suggest that they have considerable potential as a fuel.

4. Conclusions

The co-combustion characteristics of SS and CG have been investigated for the first time using a TGA and ANN model. CG addition increased DTG_{max} and the reactivity of SS. Interactions between SS and CG positively affected the combustion process and the extent of the impact varied with temperature region. When the CG proportion was increased, T_i , DTG_{max} and S increased, but T_f and M_f decreased. The minimum E_a average was obtained at CG = 40%. The agreement between ANN values and experimental data verified its ability to accurately predict co-combustion behavior provided that the heating rate, mixing ratio and temperature are known.

Acknowledgements

This work was supported by the National Natural Science Foundation of China (No. 51308132), the Science and Technology Planning Project of Guangdong Province, China (Nos. 2015B020235013; 2014A050503063; 2015A020215033), the Scientific and Technological Planning Project of Guangzhou, China (No. 201510010033, 2016201604030058) and Guangdong Special Support Program for Training High Level Talents (No. 2014TQ01Z248).

Appendix A. Supplementary data

Supplementary data associated with this article can be found, in the online version, at <http://dx.doi.org/10.1016/j.biortech.2016.11.069>.

References

- Aboukhas, A., El Harfi, K., El Bouadili, A., 2008. Pyrolysis of olive residue/low density polyethylene mixture: Part 1 thermogravimetric kinetics. *J. Fuel Chem. Technol.* 36, 672–678.
- Akahi, T., Sunose, T., 1971. Joint convention of four electrical institutes. *Sci. Technol.* 16, 22–31.
- Ata, R., 2015. Artificial neural networks applications in wind energy systems: a review. *Renew. Sustain. Energy Rev.* 49, 534–562.
- Buyukada, M., 2016. Co-combustion of peanut hull and coal blends: artificial neural networks modeling, particle swarm optimization and Monte Carlo Simulation. *Bioresour. Technol.* 216, 280–286.
- Caner, M., Gedik, E., Kecebas, A., 2011. Investigation on thermal performance calculation of two type solar air collectors using artificial neural network. *Expert Syst. Appl.* 38, 1668–1674.
- Celaya, A.M., Lade, A.T., Goldfarb, J.L., 2015. Co-combustion of brewer's spent grains and Illinois No. 6 coal: impact of blend ratio on pyrolysis and oxidation behavior. *Fuel Process. Technol.* 129, 39–51.
- Ceylan, S., Topçu, Y., 2014. Pyrolysis kinetics of hazelnut husk using thermogravimetric analysis. *Bioresour. Technol.* 156, 182–188.
- Damartzis, Th., Vamvuka, D., Sfakiotakis, S., Zabaniotou, A., 2011. Thermal degradation studies and kinetic modeling of cardoon (*Cynara cardunculus*) pyrolysis using thermogravimetric analysis (TGA). *Bioresour. Technol.* 102, 6230–6238.
- Doyle, C.D., 1961. Kinetic analysis of thermogravimetric data. *J. Appl. Polym. Sci.* 5, 285–292.
- Du, S.W., Chen, W.H., Lucas, J.A., 2014. Pretreatment of biomass by torrefaction and carbonization for coal blend used in pulverized coal injection. *Bioresour. Technol.* 161, 333–339.
- Duan, L.B., Zhao, C.S., Zhou, W., Qu, C.R., Chen, X.P., 2009. Investigation on coal pyrolysis in CO₂ atmosphere. *Energy Fuels* 23, 3826–3830.
- Flynn, J.H., Wall, L.A., 1966. A quick, direct method for the determination of activation energy from thermogravimetric data. *Polym. Lett.* 4, 323–328.
- Gai, C., Dong, Y.P., Zhang, T.H., 2013. The kinetic analysis of the pyrolysis of agricultural residue under non-isothermal conditions. *Bioresour. Technol.* 127, 298–305.
- Gajic, D., Savic-Gajic, I., Savic, I., Georgieva, O., Gennaro, S., 2015. Modelling of electrical energy consumption in an electric arc furnace using artificial neural networks. *Energy* 108, 132–139.
- Garcia, G., Aruazo, J., Gonzalo, A., Sanchez, J.L., Abrego, J., 2013. Influence of feedstock composition in fluidized bed co-gasification of mixtures of lignite, bituminous coal and sewage sludge. *Chem. Eng. J.* 222, 345–352.
- Gil, M.V., García, R., Pevida, C., Rubiera, F., 2015. Grindability and combustion behavior of coal and torrefied biomass blends. *Bioresour. Technol.* 191, 205–212.
- Goldfarb, J.L., Ceylan, S., 2015. Second-generation sustainability: application of the distributed activation energy model to the pyrolysis of locally sourced biomass-coal blends for use in co-firing scenarios. *Fuel* 160, 297–308.
- He, Y., Ma, X.Q., Zeng, G.B., 2015. Consequences of poly(vinyl chloride) presence on the thermochemical process of lignocellulosic biomass in CO₂ by thermogravimetric analysis. *Bioresour. Technol.* 177, 345–354.
- Jayaraman, H., GökulpZhou, I., 2015. Pyrolysis, combustion and gasification characteristics of miscanthus and sewage sludge. *Energy Convers. Manage.* 89, 83–91.
- Jeguirim, M., Limousy, L., Dutournie, P., 2014. Pyrolysis kinetics and physicochemical properties of aprompels produced from spent ground coffee blended with conventional biomass. *Chem. Eng. Res. Des.* 92, 1876–1882.
- Kan, T., Strezov, V., Evans, T., 2014a. Catalytic pyrolysis of coffee grounds using NiCu-impregnated catalysts. *Energy Fuels* 28, 228–235.
- Kan, T., Strezov, V., Evans, T., Kan, T., Grierson, S., de Nys, R., Strezov, V., 2014b. Comparative assessment of the thermochemical conversion of freshwater and marine Micro- and macroalgae. *Energy Fuels* 28, 104–114.
- Kim, Y.S., Kim, Y.S., Kim, S.H., 2010. Investigation of thermodynamic parameters in the thermal decomposition of plastic waste-waste lube oil compounds. *Environ. Sci. Technol.* 44, 5313–5317.
- Kissinger, H.E., 1957. Reaction kinetics in differential thermal analysis. *Anal. Chem.* 29, 1702–1706.
- Kulikowska, D., 2016. Kinetics of organic matter removal and humification progress during sewage sludge composting. *Waste Manage.* 49, 196–203.
- Li, X.F., Strezov, V., Kan, T., 2014. Energy recovery potential analysis of spent coffee grounds pyrolysis products. *J. Anal. Appl. Pyrolysis* 110, 79–87.
- Lin, L.L., Yan, R., Liu, Y.Q., Jiang, W.J., 2010. In-depth investigation of enzymatic hydrolysis of biomass wastes based on three major components: cellulose, hemicellulose and lignin. *Bioresour. Technol.* 101, 8217–8223.
- Liu, J.Y., Chen, J.C., Sun, S.Y., Kuo, J.H., Chang, K.L., Huang, S.S., Huang, L.M., Chen, N.W., Ren, J., Liu, Z.Q., 2015. Analysis of the co-combustion of sewage sludge and spent coffee grounds. *Huangjing Kexue Xuebao* 36, 3784–3794.
- López-Barrera, D.M., Vázquez-Sánchez, K., Loarca-Piña, M.G.F., Campos-Vega, R., 2016. Spent coffee grounds, an innovative source of colonic fermentable compounds, inhibit inflammatory mediators in vitro. *Food Chem.* 212, 282–290.
- López-González, D., Fernandez-Lopez, M., Valverde, J.L., Sanchez-Silva, L., 2014. Kinetic analysis and thermal characterization of the microalgae combustion process by thermal analysis coupled to mass spectrometry. *Appl. Energy* 114, 227–237.
- Lopez-Velazquez, M.A., Santes, V., Balmaseda, J., Torres-Garcia, E., 2013. Pyrolysis of orange waste: a thermo-kinetic study. *J. Anal. Appl. Pyrolysis* 99, 170–177.
- Magdziarz, A., Werle, S., 2014. Analysis of the combustion and pyrolysis of dried sewage sludge by TGA and MS. *Waste Manage.* 34, 174–179.
- Manara, P., Zabaniotou, A., 2012. Towards sewage sludge based biofuels via thermochemical conversion – a review. *Renew. Sustain. Energy Rev.* 16, 2566–2582.
- Mazrou, H., 2009. Performance improvement of artificial neural networks designed for safety key parameters prediction in nuclear research reactors. *Nucl. Eng. Des.* 239, 1901–1910.
- Mikulandric, R., Loncar, Drazen., Böhning, D., Böhme, R., Beckmann, M., 2014. Artificial neural network modelling approach for a biomass gasification process in fixed bed gasifiers. *Energy Convers. Manage.* 87, 1210–1223.
- Oleszczuk, P., 2009. Sorption of phenanthrene by sewage sludge during composting in relation to potentially bioavailable contaminant content. *J. Hazard. Mater.* 161, 1330–1337.
- Ozawa, T., 1965. A new method of analyzing thermogravimetric data. *Bull. Chem. Soc. Jpn.* 38, 1881–1886.
- Pandey, D.S., Das, S., Pan, I., Leahy, J., Kwapinski, W., 2016. Artificial neural network based modelling approach for municipal solid waste gasification in a fluidized bed reactor. *Waste Manage.* <http://dx.doi.org/10.1016/j.wasman.2016.08.023>.
- Parshetti, G.K., Quek, A., Betha, R., Balasubramanian, R., 2014. TGA-FTIR investigation of co-combustion characteristics of blends of hydrothermally carbonized oil palm biomass (EFB) and coal. *Fuel Process. Technol.* 118, 228–234.
- Peng, X.W., Ma, X.Q., Xu, Z.B., 2015. Thermogravimetric analysis of co-combustion between microalgae and textile dyeing sludge. *Bioresour. Technol.* 180, 288–295.
- Rivera, E.C., Rabelo, S.C., Garcia, D.R., Filho, R.M., da Costa, A.C., 2010. Enzymatic hydrolysis of sugarcane bagasse for bioethanol production: determining optimal enzyme loading using neural networks. *J. Chem. Technol. Biotechnol.* 85, 983–992.
- Sahin, F., 2015. Effects of engine parameters on ionization current and modeling of excess air coefficient by artificial neural network. *Appl. Therm. Eng.* 90, 94–101.
- Sahu, S.G., Chakraborty, N., Sarkar, P., 2014. Coal-biomass co-combustion: an overview. *Renew. Sustain. Energy Rev.* 39, 575–586.
- Seggiani, M., Puccini, M., Raggio, G., Vitolo, S., 2012. Effect of sewage sludge content on gas quality and solid residues produced by co-gasification in a updraft gasifier. *Waste Manage.* 32, 1826–1834.

- Simões, J., Maricato, É., Nunes, F.M., Domingues, M.R., Coimbra, M.A., 2014. Thermal stability of spent coffee ground polysaccharides: galactomannans and arabinogalactans. *Carbohydr. Polym.* 101, 256–264.
- Vamvuka, D., Salpigidou, N., Kastanaki, E., Sfakiotakis, S., 2009. Possibility of using paper sludge in co-firing applications. *Fuel* 88, 637–643.
- Vani, S., Sukumaran, R.K., Savithri, S., 2015. Prediction of sugar yields during hydrolysis of lignocellulosic biomass using artificial neural network modeling. *Bioresour. Technol.* 188, 128–135.
- Yang, H., Yan, R., Chen, H., Zheng, C., Lee, D.H., Liang, D.T., 2006. In-depth investigation of biomass pyrolysis based on three major components: hemicellulose, cellulose and lignin. *Energy Fuels* 20, 388–393.
- Yildiz, Z., Uzun, H., 2015. Prediction of gas storage capacities in mental organic frameworks using artificial neural network. *Microporous Mesoporous Mater.* 208, 50–54.
- Yildiz, Z., Uzun, H., Ceylan, S., Topcu, Y., 2016. Application of artificial neural networks to co-combustion of hazelnut husk-lignite coal blends. *Bioresour. Technol.* 200, 42–47.
- Zheng, G., Koziński, J.A., 2000. Thermal events occurring during the combustion of biomass residue. *Fuel* 79, 181–192.
- Zhou, H., Long, Y.Q., Meng, A.H., Li, Q.H., Zhang, Y.G., 2013. The pyrolysis simulation of five biomass species by hemicellulose, cellulose and lignin based on thermogravimetric curves. *Thermochim. Acta* 566, 36–43.